Supplementary information for

Evaluation of hydrometallurgical black mass recycling with simulation-based life cycle assessment

Marja Rinne[1], Riina Aromaa-Stubb[1], Heini Elomaa[2], Antti Porvali[3], Mari Lundström[1]

[1]Aalto University, School of Chemical Engineering, Department of Chemical and Metallurgical Engineering, Finland

[2]Metso, Finland

[3]VTT Technical Research Centre of Finland, Finland

Table of contents

S1. Simulation description 2

S1.1. Flowsheets in HSC Sim 2

S1.2. Leaching 6

S1.3. Solvent extraction 7

S1.4. Cementation and precipitation 8

S1.5. Crystallization 9

S1.6. Design parameters 10

S2. Heat and power consumption 12

S3. Simulation observations 13

S3.1. Products and recovery rates 13

S3.2. Solid waste 14

S3.3. Copper and iron balance 14

S4. Recommendations for further process development 16

References 17

S5. Unit specific and NMC material LCI 20

S6. Tabulated numerical results 23

S6.1. Impact characterization 23

S6.2. Contribution analysis (units) 25

S6.3. Contribution analysis (flows) 27

S1. Simulation description

The simulation module of Metso's HSC Chemistry 10 software was used for the simulation (Metso, 2023). The simulation tool is highly flexible in the modeling of a wide array of chemical engineering processes, but the embedded database makes the software most useful for mineral processing and metallurgical industries.

S1.1. Flowsheets in HSC Sim

The flowsheets were identical aside from the manganese recovery and iron removal parts. Figure S1 represents the leaching circuit, Figure S5 cobalt, nickel, and lithium recovery, and Figure S6 effluent treatment, which are shared between the flowsheets. Figures S2, S3, and S4 represent the scenario-specific manganese recovery and iron and aluminum removal stages. The main steps in the processes were reducing leaching with sulfuric acid, copper cementation, iron and aluminum hydrolysis, solvent extraction (SX) and oxidative precipitation of manganese, the respective SX and crystallization of cobalt sulfate heptahydrate and nickel sulfate hexahydrate, sodium sulfate crystallization, lithium carbonate precipitation, and the final effluent treatment.

SX was selected as the main solution purification method due to its wide-spread industrial implementation in the separation of particularly copper, nickel, and cobalt bearing solutions. The extractants were commonly used ones: di-(2-ethyl hexyl) phosphoric acid (D2EHPA) for manganese and nickel, and bis (2,4,4-trimethylpentyl) phosphinic acid (Cyanex 272) for cobalt. The extractants were diluted with sulfonated kerosene, and tributyl phosphate (TBP) was used as the modifier. SX consists of two main steps: extraction, where the impure solution is contacted with the organic to selectively extract the target metal and then the two phases (raffinate and loaded organic) are physically separated due to their immiscibility, and stripping, where a suitable aqueous phase is used to extract the metal from the organic phase. Extraction and stripping may both require multiple, usually counter-currently operated mixer-settler systems to reach optimal separation and recovery efficiencies, but the flowsheets were modeled with only a single unit for each extraction, stripping, and organic washing step as shown in the following figures.

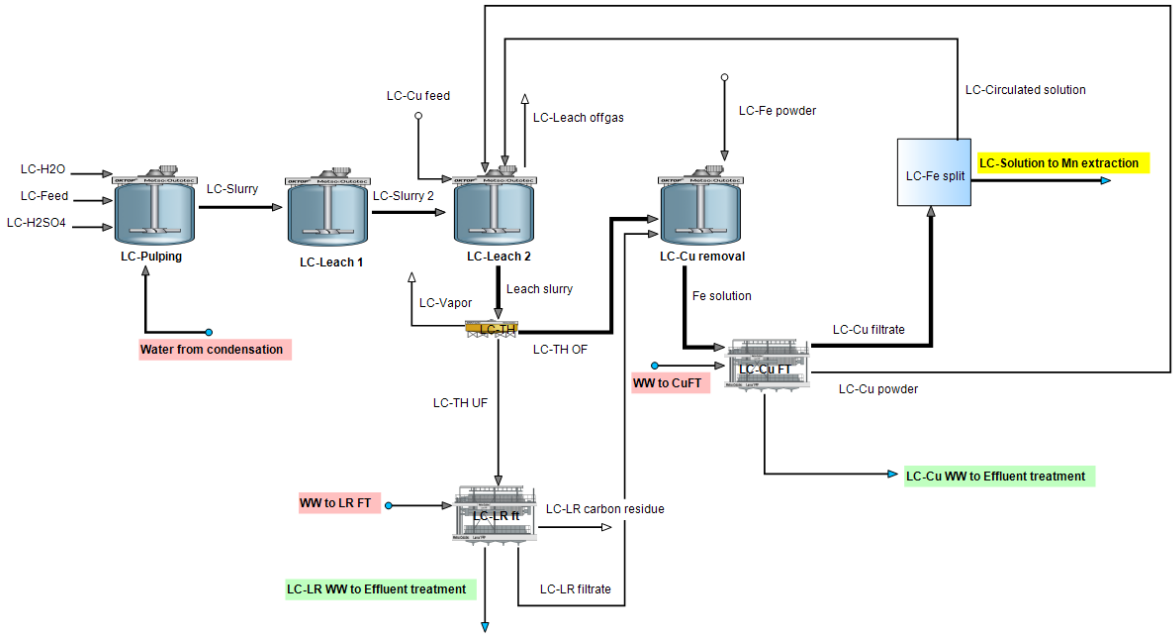

Figure S1. The leaching circuit (LC) flowsheet drawn in HSC Sim. Flows coming from or entering other sections of the flowsheet are highlighted with colors. Bright yellow highlight: to manganese circuit, light green highlight: to effluent treatment, light red highlight: water from nickel, cobalt, and lithium circuits.

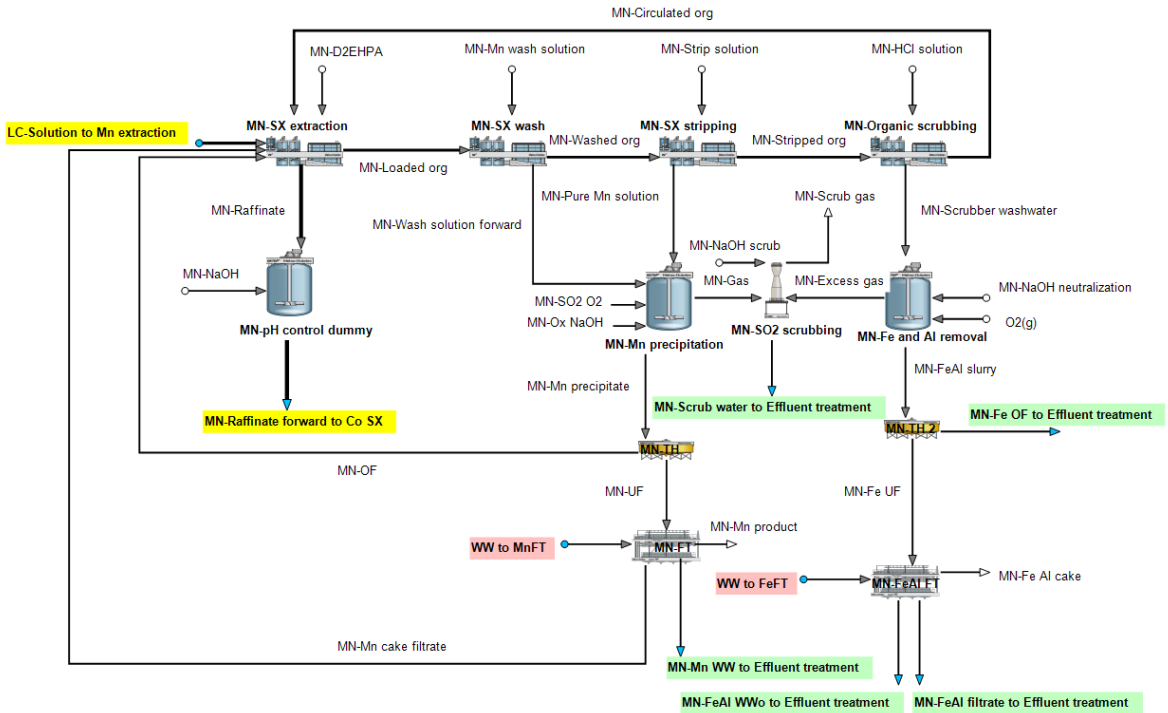

Figure S2. Manganese refining and iron removal stages in *FS1*. Inflow from leaching circuit and the outflow to cobalt extraction are highlighted with yellow, inflows from condensation with light red, and outflows to effluent treatment with light green.

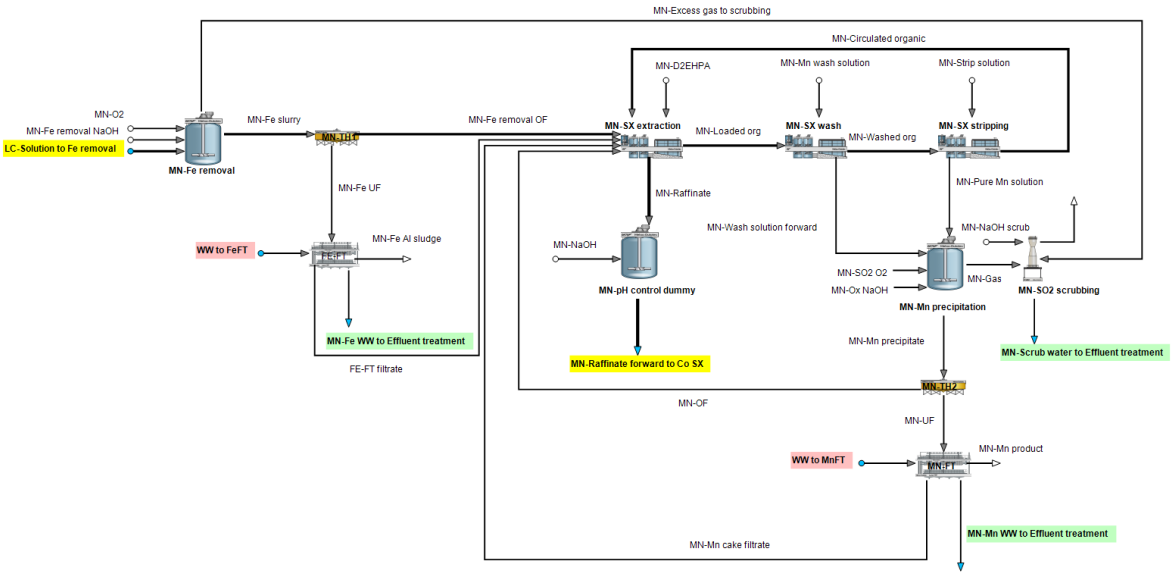

Figure S3. Manganese refining and iron removal stages in *FS1*. Inflow from leaching circuit and the outflow to cobalt extraction are highlighted with yellow, inflows from condensation with light red, and outflows to effluent treatment with light green.

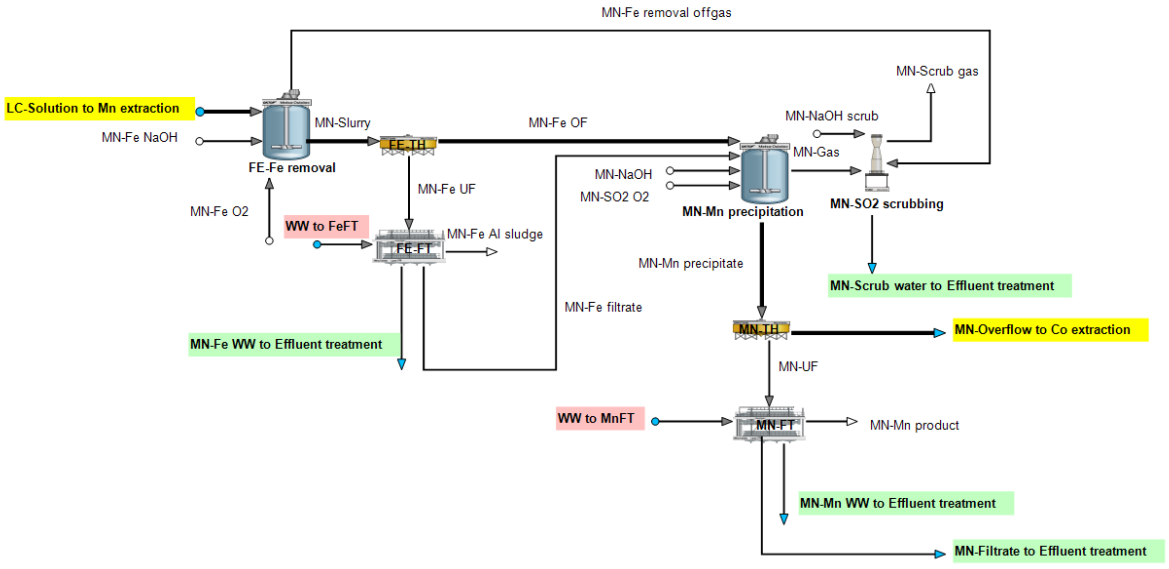

Figure S4. Manganese refining and iron removal stages in *FS2*. Inflow from leaching circuit and the outflow to cobalt extraction are highlighted with yellow, inflows from condensation with light red, and outflows to effluent treatment with light green.

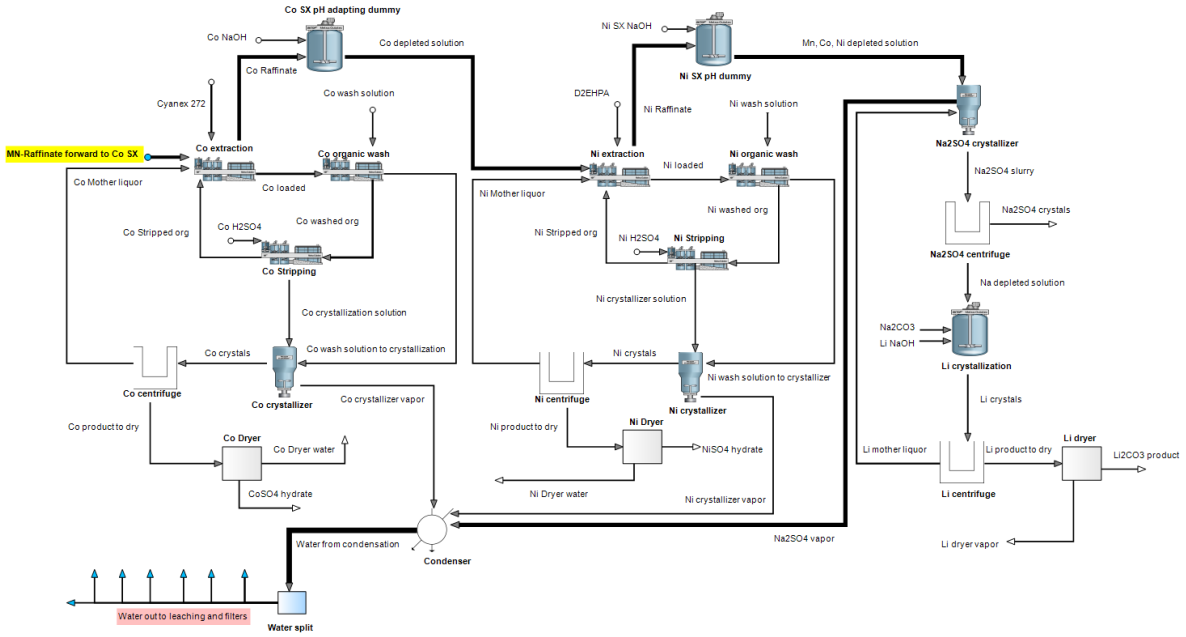

Figure S5. Cobalt, nickel, and lithium recovery stages in all scenarios (*FS1-3*). Inflow from manganese refining and iron removal is highlighted with yellow, and condensation water feeds to other flowsheets with light red.

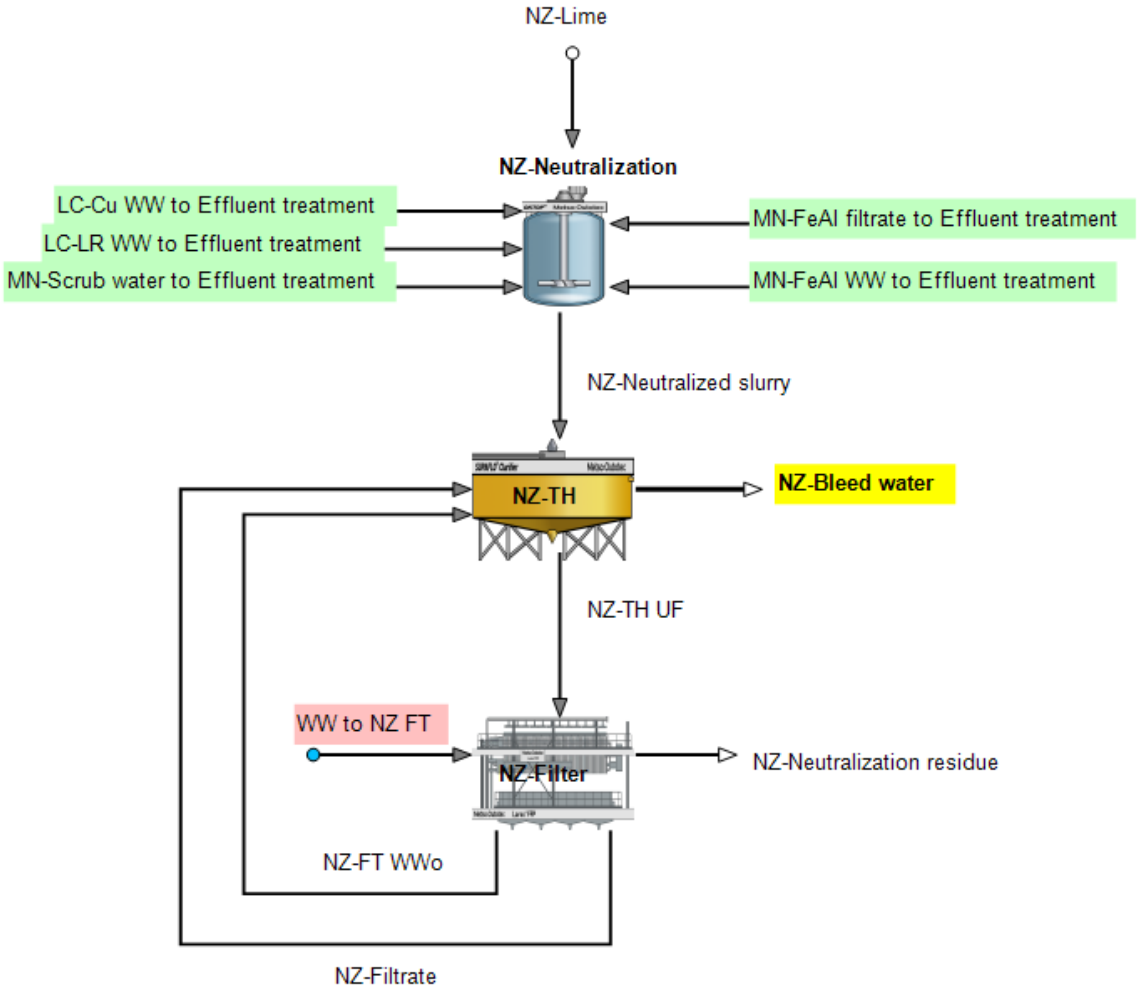

Figure S6. Final neutralization and treatment of the wastewaters in all of the scenarios (*FS1-3*). Filter wash water originating from the condensation step is highlighted with light red, the neutralized inflows from other sections of the flowsheet with light green, and the final bleed water flow with bright yellow.

S1.2. Leaching

The studied raw materials are complex mixtures of inert materials (graphite), metals (copper, iron, aluminum), cathode metal oxides, and traces of polymers and electrolyte. The overall performance of the leaching system is thus dependent on the interaction between several components and simultaneously occurring mechanisms. Experimental studies demonstrate that the extractions of lithium and cobalt are typically in the range of 80-90% and 60-70% in the absence of a reductant (Meshram et al., 2016; Joulié et al., 2017; Sun and Qiu, 2011) Joulíe et al. (2017) also showed that NMC materials may be reduced by metallic copper and aluminum foils alone, which is also backed by the findings of Chernyaev et al. (2021a) on cobalt-rich industrial waste. The latter study also confirmed that dissolved iron does significantly enhance leaching kinetics of industrial raw materials together with copper or aluminum.

The leaching kinetics of synthetic lithium cobalt oxide (LCO) in the presence of copper and dissolved iron have been modeled by Porvali et al. (2020a), and the model was used to predict the leaching extractions in the second leaching setup in the simulation model. The retention time was set at 120 min, and the extractions were calculated based on the solid copper (Cu(s)) and iron(II) amounts in the system. 80% of iron(III) was assumed to regenerate to iron(II) in contact with copper, and the leaching extraction of metallic copper thus mainly depended on the amount of iron in the system. Oxygen generated by the dissolution of the cathode materials without reductant was assumed to have a very limited effect on the system. The simulation is thus only applicable for cases where the amount of copper is sufficient to regenerate the reductant iron(II). The dependency between leaching extraction and the amounts of iron and copper in the system may be described as follows, Eq. (S1) (Porvali et al., 2020):

$$X_{LiMeO_2}(t = 120\ \text{min}) = 100\% \cdot 120\ \text{min} \cdot (1 - \left(1 - k_c([Fe], [Cu])\right)^{1/3}) \quad \text{(S1)}$$

where X_{LiMeO2} is the extraction of $LiMeO_2$ (%), k_c is the reaction rate constant (unit), which is dependent on [Fe] and [Cu]. [Fe] is the mol ratio of iron in the system vs. $LiMeO_2$ (mol/mol), and [Cu] is the mol ratio of metallic Cu in the system vs. $LiMeO_2$ (mol/mol).

Based on the model of Porvali et al. (2020a), the mol ratios of copper and iron to the active materials ($LiCoO_2$, $LiMnO_2$, $LiNiO_2$) were adjusted to 0.6 and 0.11, respectively. It was hence assumed that similar conditions are optimal for the dissolution of complex mixtures of cathode materials. Direct interaction between the active materials and the copper and aluminum foils are also possible, but the iron catalyzed route is assumed more likely at relatively short retention times (120 min). The effect of metallic aluminum, as discussed in the studies of Joulíe et al. (2017) and Chernyaev et al. (2021a), was also ignored.

$LiNiO_2$, $LiCoO_2$, and $LiMnO_2$ were presumed to dissolve at equivalent rates at the conditions, which causes some error, and the leaching model could be improved with experimental data on industrial raw materials. The value of the model, however, lies in studying the effect of such variation in the solution circulation, inputs, and outputs, rather than in the individual process units.

S1.3. Solvent extraction

In the previous study by Rinne et al. (2021), the solvent extraction steps were modeled with a black box approach, where extraction and stripping were combined into a single step without any organic phase. In the current model, extraction and stripping were simulated separately with the organic flow.

The missing organic-metal complexes were therefore added to the user specific database in HSC Sim to be used in the reactions between the extractant and the metal ion. The extraction and stripping reactions were thus implemented in the model, unlike in the previous black box interface. For

example, the extraction and stripping of aqueous manganese in D2EHPA may be described by reversible reaction (S2). The stripping reaction occurs in the reverse order.

$$\mathrm{Mn}^{2+}(aqueous) + \mathrm{RH}_2(organic) \leftrightarrow \mathrm{RMn}(organic) + 2\mathrm{H}^{+}(aqueous) \quad \text{(S2)}$$

Scrubbing steps were modeled where applicable. Two-step scrubbing was implemented for the organic in manganese solvent extraction *FS1* and one-step scrubbing in *FS2*. In the first step, co-extracted lithium, cobalt, and nickel were removed with the purified manganese sulfate solution (O/A 10:1, $[Mn^{2+}]$ = 4 g/L). The once scrubbed organic was then treated to remove iron and aluminum from the organic, which is challenging even with concentrated acids (Lupi and Pilone, 2000). Hydrochloric acid solution (6 M) was used by Peng et al. (2019), but oxalic acid has also proven successful (Singh et al., 2013). Due to the need for highly concentrated acid, minimizing iron in the feed solutions may be desirable from an industrial standpoint, and the use of iron in copper cementation could be hypothesized to potentially cause problems in Mn extraction.

The cobalt and nickel bearing organics were likewise scrubbed by splitting the purified solution flows between crystallization and the respective scrubbing steps and diluting the flow with water to obtain 0.3 g/L aqueous cobalt and nickel sulfate washing solutions at 5:1 O/A ratios. While Liu et al. (2019) did not specify the washing of Cyanex 272, the step was regardless implemented into the simulation with the parameters used in the washing of D2EHPA in nickel extraction.

This “grey box” approach to solvent extraction makes it easier to implement further details to the model, such as crud formation, droplet entrainment, and organic scrubbing steps. The method, however, still requires experimentally determined or supplier provided data, such as organic/aqueous phase ratios, impurities, and extractant loading capacities.

S1.4. Cementation and precipitation

Simple models were used for the cementation, precipitation, and neutralization steps mainly based on experimental results or estimations. It was, for instance, assumed that 99% dissolved copper may be removed from the solution as metallic copper with the addition of a stoichiometric amount of iron.

Iron and aluminum removal in *FS2* and *FS3* were based on the work of Chernyaev et al. (2021b) assuming that aluminum would be 2 g/L at maximum. At pH 4, cobalt and nickel losses were approximately 2% and 1%, whereas 2% lithium was lost. The iron and aluminum rich hydrochloric acid solution was treated by neutralization to hydrolyze the metals in *FS1*.

The data for manganese dioxide (MnO_2) precipitation was obtained from the work of Zhang et al. (2002), who observed that approximately 100% of manganese may be precipitated from solution with sulfur dioxide and oxygen (SO_2/O_2) gas mixtures. The oxidation of divalent Mn^{2+} to quadrivalent Mn^{4+} is slow with oxygen alone, and the oxidation reaction (S3) is catalyzed by sulfur dioxide. At optimal conditions in laboratory scale, the vol.% of sulfur dioxide in the gas was 5.7, and the kinetics

improve when the pH increases. In the absence of cobalt and nickel in the solution, which begin to significantly co-precipitate at pH>4, pH mainly affects the oxidation rate of manganese and thus the retention time. It was assumed in the current work that manganese is precipitated at 80 °C, pH 3, and that three times the stoichiometric amount (reaction S3) of oxygen is consumed. The excess sulfur dioxide gas was neutralized with sodium hydroxide solution.

$$2MnSO_4(aq) + O_2(g) + 2H_2O \rightarrow 2MnO_2(s) + 2H_2SO_4(aq) \quad \text{(S3)}$$

All the effluents in the process were directed to final neutralization, where all the remaining dissolved metallic impurities (aside from calcium, lithium, and sodium) were presumed to be removed in the final neutralization at pH 7. Trace amounts of metals should, however, be expected to be present in the neutralization discharge. Of the components found in waste lithium-ion batteries, the elements capable of most harm to the environment are nickel, cobalt, fluoride, and copper, but large concentrations of less hazardous sodium and sulfate are also going to be present.

Only the most concerning toxic metal cations copper, cobalt, and nickel, and sulfate and chloride were included in the calculations. Sulfate and chloride have no impacts in the used CML v.4.8 2016 method, but both anions are significant because of their indirect effects in freshwater environments. It should be also noted that fluoride was not included despite its hazards, since it was not analysed from the raw material. Fluoride removal in recycling processes is, nonetheless, the topic of several studies due to its dangers.

Only the amounts of copper, cobalt, and nickel in the wastewaters were given estimates. The solubilization of metals from solid residues, such as leach and neutralization residues, is more challenging to include without standardized tests. The solubility of transition metal hydroxides in circumneutral solutions is generally very low (Dyer et al., 1998).

S1.5. Crystallization

It was assumed that mechanical vapor recompression (MVR) technology would be used in the crystallizers, although no rigorous crystallizer design was conducted with HSC Sim, and only an estimate of the mass and heat balance could be provided. The condensed vapor is used in pre-heating the feed and returned to the process to minimize water consumption. The evaporators were estimated to consume 10 kWh electricity for 1 m^3 of condensed vapor (Hankins and Singh, 2016).

The models applied in nickel and cobalt crystallization were previously reported by Rinne et al. (2021) without the application of copper control to evaporate water due to the lack of copper in the feed solutions. Instead, it was set that a certain percentage of water (90%) is evaporated, and cobalt sulfate heptahydrate ($CoSO_4 \cdot 7H_2O$) and nickel sulfate hexahydrate ($NiSO_4 \cdot 6H_2O$) crystallize from the concentrated sulfuric acid solutions based on their solubilities, as reported by Charykova et al. (2010) and Kobylin et al. (2013). The crystals are separated from the mother liquor and washed with

centrifuges, and the wash solution and mother liquor are circulated back into solvent extraction steps to maximize the recovery of cobalt and nickel. The temperature in the crystallization step was presumed 60 °C, and the crystallization occurs under vacuum.

In sodium sulfate crystallization step, water was evaporated to leave a discharge solution containing 20 g/L lithium. The degree of sodium sulfate crystallization was controlled by its solubility at 80 °C, which is approximately 45 wt.% water (Linke, 1964). The crystals were separated before lithium carbonate crystallization, where sodium carbonate was fed at stoichiometric quantities. Like with the other crystallization products, the yield of lithium carbonate was defined based on its solubility, which was estimated 9.6 g/L (1.8 g/L Li^+) at 80 °C (An et al., 2012). The centrifugation and washing of the crystals were modeled with the ready thickener models found in HSC Sim with a wash water feed to approximate the water balance. The mother liquors were returned to the process: cobalt and nickel liquors to their respective solvent extraction stages, and lithium liquor to sodium sulfate crystallization. After centrifugation, the product crystals were dried at low temperature (80 °C).

S1.6. Design parameters

The simulation model was constructed with process parameters found in the literature for each of the process steps, as may be seen in Table S1. There parameters were used in controlling model variables and inputs in the simulation. Thickeners and filters were modeled with the constants inbuilt in the ready models in HSC Sim.

Table S1. Design parameters with which the simulation controls were set.

Leaching	**Unit**	**Value**	**Reference**
$Cu/2LiMeO_2$ ratio	mol/mol	1.2	Porvali et al. (2020a)
$Fe/LiMeO_2$ ratio	mol/mol	0.11	Porvali et al. (2020a)
H_2SO_4 concentration	mol/L	2.0	Porvali et al. (2020a)
pH after leaching (only FS2-LA)	-	1.89	Porvali et al. (2020b)
S/L ratio	g/L	100	
Mn solvent extraction	**Unit**	**Value**	**Reference**
pH	-	3.2	Peng et al. (2019)
O/A ratio in extraction	vol/vol	2:1	Peng et al. (2019)
O/A in stripping	vol/vol	8:1	Peng et al. (2019)
Extractant in organic	mol/L	4	Peng et al. (2019)
H_2SO_4 concentration in stripping	pH	4	Peng et al. (2019)
Mn concentration in scrubbing (1)	g/L	4	Peng et al. (2019)
HCl concentration in scrubbing (2)	mol/L	6	Peng et al. (2019)
O/A ratio in scrubbing (1)	vol/vol	10	Peng et al. (2019)
O/A ratio in scrubbing (2)	vol/vol	0.1	Peng et al. (2019)
Mn precipitation	**Unit**	**Value**	**Reference**
SO_2 partial pressure in SO_2/O_2	p.%	6	Zhang et al. (2002)
pH	-	3–4	Zhang et al. (2002)
O_2 utilization efficiency	%	33	Estimate
Al and Fe removal	**Unit**	**Value**	**Reference**
pH in neutralization	-	4	Chernyaev et al. (2021b)
Co solvent extraction	**Unit**	**Value**	**Reference**
pH	-	5.5	Liu et al. (2019)
Co loading in extractant	g/L	~17	Rinne et al. (2021)
O/A in extraction	vol/vol	1:1	Liu et al. (2019)
O/A in stripping	vol/vol	5:1	Liu et al. (2019)
Extractant in organic	vol.%	20	Liu et al. (2019)
H_2SO_4 concentration in stripping	mol/L	1	Liu et al. (2019)
$CoSO_4$ concentration in scrubbing	mol/L	0.3	Estimate
Ni solvent extraction	**Unit**	**Value**	**Reference**
pH	-	6	Liu et al. (2019)
O/A in extraction	vol/vol	1:2	Estimate, Liu et al. (2019)
O/A in stripping	vol/vol	2.5:1	Estimate, Liu et al. (2019)
Extractant in organic	vol.%	25	Liu et al. (2019)
H_2SO_4 concentration in stripping	mol/L	1	Liu et al. (2019)
O/A in scrubbing	vol/vol	5:1	Liu et al. (2019)
$NiSO_4$ concentration in scrubbing	mol/L	0.3	Liu et al. (2019)
Sodium sulfate crystallization	**Unit**	**Value**	**Reference**
Li concentration	g/L	20	An et al. (2012)
Na_2SO_4 solubility	g/L	12	An et al. (2012)
Lithium carbonate crystallization	**Unit**	**Value**	**Reference**
Li concentration	g/L	1	An et al. (2012)
pH	-	12	An et al. (2012)

S2. Heat and power consumption

The electricity mix used in the LCA was assumed to be EU average in 2020, which was compiled from the EU 2020 reference scenario (European Commission, 2021). The mix assumes 25% nuclear, 14% coal, 1% oil, 19% natural gas, 6% biomass, 13% hydropower, 15% wind power, and 6% solar. The share of renewable fuels was consequently 40% in electricity generation. Heat for the crystallizers was assumed to be generated with steam in chemical industry.

While the heat balance may be approximately calculated with HSC Sim, the software does not estimate the electricity consumption in the process. The power consumption is calculated based on the mass balance by dimensioning the largest key equipment: reactors, thickeners, filters, and evaporators and crystallizers. Various ancillary equipment, such as pumps and lights, are included in the form of a general constant (1-2 MW) depending on the throughput. 1 MW was presumed a safe estimate for 10 t/h feed. The methodology has previously been described in detail by Elomaa et al. (2020) and Rinne et al. (2021). Centrifuges were assumed to consume 1 kWh for 1 m^3 feed (Szepessy and Thorwid, 2018).

The experimental data used in the model is obtained from batch tests, but the process is presumed to run continuously or semi-continuously in industrial scale, which leads to some error in the estimated retention times. The process was also simulated in steady state, leading to similar types of issues. Buffer tanks, for instance, were not accounted for in the energy consumption. The error is mainly expected to affect the energy consumption of the process units, but possibly also the accumulation of impurity elements particularly in solvent extraction. The error in energy consumption has obvious effects on the environmental impacts of the process, but the significance of this also depends on the environmental intensity of energy production.

The heat balance is more difficult to assess than the mass balance due to the steady-state nature of the simulation. Heat losses through evaporation and conduction to reactor and equipment walls were not accounted for in any process units aside from the crystallization steps, where the temperature was the closest to the boiling point of water. The reactions in leaching, neutralization, and manganese precipitation are exothermic, but cobalt, nickel, and lithium recovery are heat consuming.

There is little industrial data on the energy consumption of hydrometallurgical black mass processing, since the processes are new and not highly energy intensive. Some references and existing data points could be used for comparison to assess if the value is in acceptable range. Mohr et al. (2021) estimated the electricity consumption of treating 1 kg pre-treated battery cells to be 0.14 kWh in their LCI. In the present study, the estimate is 0.38-0.42 kWh for 1 kg black mass, which corresponds to approximately 0.14 kWh for 1 kg cells. No other energy sources were included in the LCI.

S3. Simulation observations

Battery recycling process simulation in the current study was used in investigating recycled battery metal product recoveries and purities as well as process waste compositions.

S3.1. Products and recovery rates

Products considered in the study were nickel sulfate hexahydrate ($NiSO_4 \cdot 6H_2O$), cobalt sulfate heptahydrate ($CoSO_4 \cdot 7H_2O$), lithium carbonate (Li_2CO_3), and manganese dioxide (MnO_2). Additionally, metallic copper was recovered for re-use in the process. The simulated recoveries and product purities are reported in Table S2. The purities may be overly optimistic particularly with lithium, which was extracted last. Re-crystallization can improve lithium carbonate (also nickel and cobalt sulfate) purity if needed, or the products can be fed to existing processes as intermediate products.

Best final recoveries were obtained in *FS1*, where manganese was extracted directly by SX, leaving nickel, cobalt, and lithium to be recovered from raffinate without losses to the manganese product or neutralization sludge. The high solubility of lithium carbonate could be overcome by circulating the depleted mother liquor back to the evaporation process. This increases lithium recovery but results also in higher amount of solution in the circulation. In *FS3*, some nickel and cobalt were incorporated to the manganese precipitate, leading to reduced recoveries. *FS2* was a compromise solution, which achieved both reasonable recovery and purities.

Table S2. Recoveries and purities of recovered metal products in hydrometallurgical black mass treatment.

	Valuable metal recovery (%)				**Product purity (%)**			
	FS1	***FS2***	***FS3***	***F2-LA***	***FS1***	***FS2***	***FS3***	***FS2-LA***
Manganese dioxide	97.1	94.8	94.8	86.4	93.1	97.0	68.2	96.8
Cobalt sulfate	97.2	94.9	92.0	86.3	99.7	99.7	99.8	99.8
Nickel sulfate	94.6	92.3	91.0	83.1	99.4	99.4	99.4	99.4
Lithium carbonate	87.4	85.2	86.0	80.9	99.1	99.3	98.3	99.1

The proposal for the new EU regulatory framework for batteries (COM/2020/798) includes recovery targets for cobalt, nickel, copper, and lithium (European Commission, 2020). According to the proposal, >95% of nickel, copper, and cobalt, and >70% of lithium should be recovered from lithium-ion batteries by 2030. Even without accounting for the losses in pre-treatment, the 95% target for the base metals appears extremely challenging. 70% lithium, on the other hand, is undoubtedly difficult but does not seem unrealistic.

S3.2. Solid waste

Aluminum, iron, and carbon were not recovered in the current flowsheet, i.e., they end up in the solid waste streams. In addition, the used chemicals introduce species to the solution that need to be managed throughout the process.

In the leaching treatment of 1 kg of black mass, approximately 0.6 kg of solid material remained undissolved. The main constituent of this leach residues was carbon (98.6%), with only minor amounts of metals and cathode metal oxides. In theory, this residue could act as a possible feed material in the production of carbon materials after the washing and removal of the trace metals, but this is not a proven industrial process concept yet. The recycling of anode materials has garnered both academic and industrial interest, and there could be environmental benefits from this (Rey et al., 2021). The recovery of the carbon materials was, however, out of the scope of the current work.

Dissolved iron, aluminum, and traces of valuable metals were removed as mixed hydroxides by neutralizing the solution. In this process approximately 0.2 kg of neutralization residues was produced for 1 kg of feed material. The hazardousness of this waste needs to be further verified in standardized leachability tests.

The most significant waste product from the hydrometallurgical process was found to be sodium sulfate, or glauber salt ($Na_2SO_4 \cdot 10H_2O$). 3.4-3.5 kg of crystallized salt was produced for 1 kg feed material. The high amount can be explained by the use acidic sulfate media and consequent need of neutralization with caustic soda in the solvent extraction stage, which introduces sulfate and sodium into the solution. The disposal of salt waste in common landfills is prohibited, which makes the high volume of the crystallized glauber salt a risk for the feasibility process, and suitable applications are needed. Suggested possibilities for sodium sulfate management include its use in steel pickling and conversion to more valuable products, such as potassium sulfate or sodium hydroxide and sulfuric acid (Nowak et al., 2014; Ogedengbe et al., 2020; Tuovinen et al., 2021).

S3.3. Copper and iron balance

The flowsheets were identical until copper cementation, and therefore there are no differences between copper and iron consumption in the scenarios *FS1-FS3*. Ideally, copper and iron would be supplied to the process in entirety as impurities in the feed materials. However, the raw material alone is unlikely to have the necessary amount of copper and iron as 0.15 kg of copper and 0.03 kg iron is required in the leaching of 1 kg black mass (Figure S7). Therefore, a novel approach of internal reductant circulation was applied for the flowsheet - iron being recycled in dissolved form and copper in metallic form. Copper can also be supplied to the process by other types of copper scrap, such as pre-production scrap from battery manufacturing.

The model predicts that only 46% copper dissolves during leaching because some of the active materials react directly with acid, which leaves an insufficient amount of ferric iron to fully oxidize

copper. While dissolved copper can be efficiently recovered for re-use through cementation, but low leaching extraction leads to a situation where 0.09 kg of copper needs to be continuously be supplied to the process for 1 kg feed material. Iron introduced to the solution by cementation can also be utilized in the leaching step. The former is likely unfeasible, whereas the latter could be achieved by oxygen bubbling to oxidize ferrous to ferric iron. In such a case where 95% of the previously undissolved copper would be extracted to solution, only 0.006 kg of additional copper would be needed to maintain the equilibrium.

Ideally, copper in the black mass alone could sustain the leaching process without an external source, but the process requires a considerable amount of copper. The process is only feasible if the utilization of copper is optimized. 0.09 kg copper for 1 kg black mass corresponds to 8.77% copper in the raw material, whereas 0.006 kg copper to only 0.48% copper.

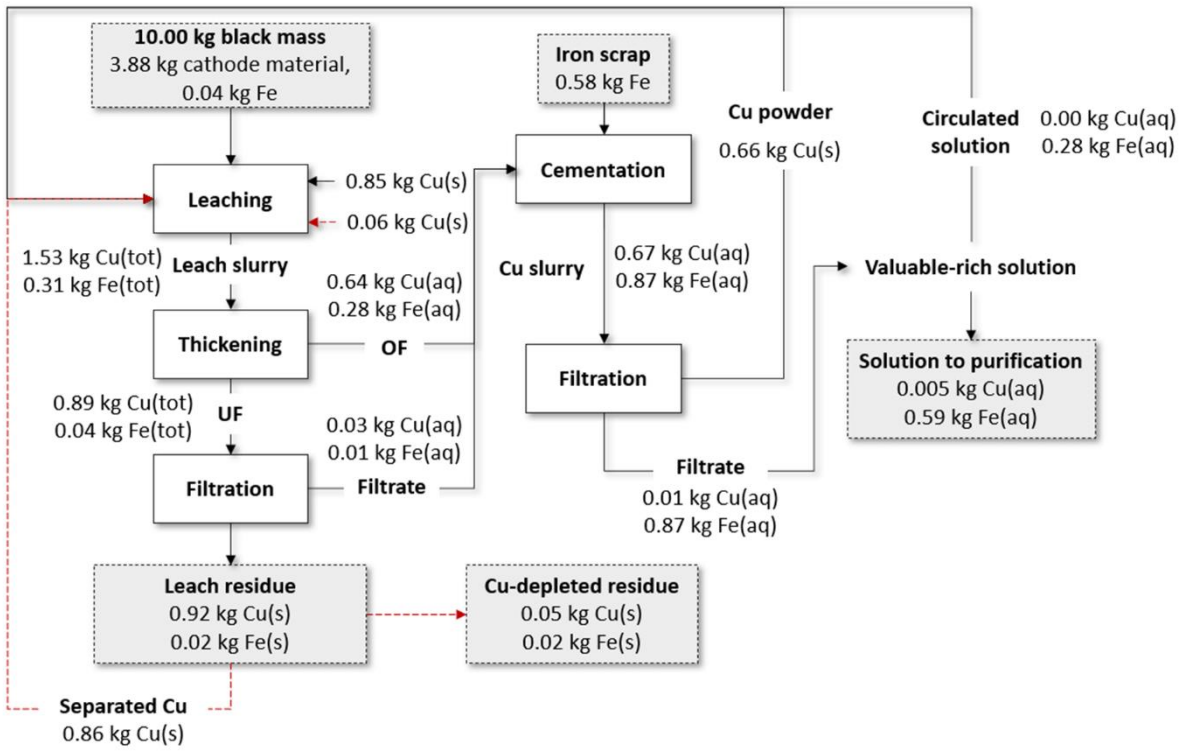

Figure S7. Mass balance of copper and iron in the process for 10 kg black mass, filter wash waters not included. The effect of separating 95% undissolved copper is highlighted with a red dashed line.

Depending on the size of the fraction, industrial black masses may contain copper from less than 1% to over than 15% (Chernyaev et al., 2022), indicating that this could be achievable. Furthermore, a high copper content in black mass is typically linked also with high aluminum content, which is undesirable in all hydrometallurgical circuits. The results, however, highlight that the process could be operable with most black masses in the absence of other copper scrap if copper circulation is adequately optimized. The main advantage of the leaching concept is that iron beneficially affects the

kinetics and copper dissolution at low concentrations (<3 g/L), which simplifies downstream processing.

S4. Recommendations for further process development

Early and detailed process evaluation was used in the work to identify the most impactful ways to reduce the environmental burden and maximize the benefits from recycling waste lithium-ion batteries. Several data gaps could be recognized by a combination of literature review, process simulation, and life cycle assessment, which also enabled the identification of the most impactful ways to reduce the environmental footprint of hydrometallurgical black mass processing. The most energy intensive steps were the crystallization stages, so the most impactful strategy to reduce the process burdens would be to maximize valuable recoveries while minimizing chemical consumption.

Some key focus areas for further development are suggested in **Table 3** based on the observations made in the earlier sections. The first three recommendations are mainly applicable for the studied leaching system, although the optimization of leach solution acidity can also be conducted with other reductants. The other suggestions are more general observations of the needs of black mass processing. For instance, the recovery of manganese and anode materials has received significantly less attention than lithium, cobalt, and nickel, and questions remain about obtaining high quality products from them. Plastics, copper, and potentially aluminum are recoverable already during pre-treatment.

Table S4. Key goals for further black mass process development by experimental work, their significance for the process or the quality of the simulation data, and the overall effect on black mass processing.

Experimental goal	Significance for the process or the model	Predicted effect
Optimize leaching time at low acid concentrations	Mild acidity decreases chemical consumptions, less salt waste is generated	Reduces impacts, lower waste burden
Study low acid leaching with industrial black mass	Confirming if phenomena observed with pure reagents applies in more complex systems	Improves the model, technical benefits
Study NMC and NCA leaching with Fe and Cu	Kinetic model used in the simulation is for pure LCO	Improves the model
Sodium sulfate valorization	Not landfillable, generated in large amounts in sulfuric acid-based processing	Lower waste burden
Study the degradation of organics	Extractants have a large impact in the process, organic losses are only an estimate	Improves the model
Further focus on manganese recovery	Manganese is difficult to selectively recover, manganese SX is not a proven process	Lower waste burden, technical benefits
Aluminum separation during pre-treatment	Aluminum forms amorphous gels, not desired in the hydrometallurgical process, energetically intensive metal to produce from ores	Technical benefits, avoided primary material production
Investigation on fluoride behaviour in the process	Binder and electrolyte behaviour was excluded from the model, hazardous element	Improves the model, safety aspects

References

An J. W., Kang D. J., Tran K. T., Kim M. J., Lim T., Tran T., 2012. Recovery of lithium from Uyuni salar brine, Hydrometallurgy, vol. 117-118. pp. 64-70. DOI: 10.1016/j.hydromet.2012.02.008

Andre D., Kim S., Lamp P., Lux S. F., Maglia F., Paschos O., Stiaszny B., 2015. Future generations of cathode materials: an automotive industry perspective, J Mater Chem A, vol. 3. pp. 6709-6732. DOI: 10.1039/C5TA00361J

Charykova M. V., Krivovichev V. G., Depmeier W., 2010. Thermodynamics of Arsenates, Selenites and Sulfates in the Oxidation Zone of Sulfide Ores. II. Systems M1, M2//SO_4^{2-} - H_2O (M1, M2=Fe^{2+}, Fe^{3+}, Cu^{2+}, Zn^{2+}, Pb^{2+}, Ni^{2+}, Co^{2+}, H^+) at 25 ^oC. Geology of Ore Deposits 52(8). Pp. 701–710. DOI: 10.1134/S1075701510080027.

Chernyaev A., Partinen J., Klemettinen L., Wilson B. P., Jokilaakso A., Lundström M., 2021a. The efficiency of scrap Cu and Al current collector materials as reductants in LIB waste leaching, Hydrometallurgy, vol. 203. DOI: 10.1016/j.hydromet.2021.105608

Chernyaev A., B. P. Wilson, M. Lundström, 2021b. Study on valuable metal incorporation in the Fe-Al precipitate during neutralization of LIB leach solution, Sci Rep, vol. 11. DOI: 10.1038/s41598-021-02019-2

Dyer J. A., Scrivner N. C., Dentel S. K., 1998. A practical guide for determining the solubility of metal hydroxides and oxides in water, Environ Prog, vol 17:1. DOI: 10.1002/ep.670170112

European Commission, 2021. EU Reference Scenario 2020 : Energy, transport and GHG emissions – Trends to 2050, Publications office. DOI: 10.2833/35750

Forte F., Pietrantonio M., Pucciarmati S., Puzone M., Fontana D., 2020. Lithium iron phosphate batteries recycling: An assessment of current status, Crit Rev Environ Sci Technol, vol. 51:19. pp. 2232-2259. DOI: 10.1080/10643389.2020.1776053

Hankins N. P., Singh R., 2016. Emerging Membrane Technology for Sustainable Water Treatment. Amsterdam: Elsevier.

Harpprecht C., van Oers L., Northey S. A., Yang Y., Steubing B., 2021. Environmental impacts of key metals' supply and low-carbon technologies are likely to decrease in the future, J Indust Ecol, vol. 25:6. pp. 1543-1559. doi: 10.1111/jiec.13181

Joulié M., Billy E., Laucournet R., Meyer D., 2017. Current collectors as reducing agent to dissolve active materials of positive electrodes from Li-ion battery wastes, Hydrometallurgy, vol. 169. pp. 426-432. DOI: 10.1016/j.hydromet.2017.02.010

Kauranen P., Kojo I. V., Salmi O., Vassart A., Lundström M., Sayfritz S., Wiesner E., Trap V., Forte F., Faucheux V., Sygmunt M., Tomboy W., Bazin J., Hilario F., Kinnunen P., Pereira B., Pettit C., Van der Eijk C., Roschger P., Berruti C., Gonzales Ramon N., Miguez J. M., Philippot M., Capiglia C., Witomski A., Hakanen E., Ibañez A., Le Petit Y., 2021. *Roadmap on Raw Materials and Recycling*, Batteries Europe WG2, European Commission. Available at: https://energy.ec.europa.eu/roadmap-raw-materials-and-recycling_en [Accessed 19 April 2022]

Kim Y., Seong W. M., Manthiram A., 2021. Cobalt-free, high-nickel layered oxide cathodes for lithium-ion batteries: Progress, challenges, and perspectives, Energy Storage Mater, vol. 34. pp. 250-259. DOI: 10.1016/j.ensm.2020.09.020

Kobylin K. P., Sippola H., Taskinen P. A., 2013. Thermodynamic model for acidic Ni(II) sulfate from solubility data, Calphad, vol. 40. pp. 41–47. DOI: 10.1016/j.calphad.2012.10.002

Lander L., Cleaver T., Rajaeifar M. A., Nguyen-Tien V., Elliott R.J.R., Heidric O., Kendrick E., Edge J. S., 2021. Financial viability of electric vehicle lithium-ion battery recycling, iScience, vol. 24, doi: 10.1016/j.isci.2021.102787

Linke W. F., 1964. Solubilities: Inorganic and metal-organic compounds, American Chemical Society, 4th ed.

Liu C., Lin J., Cao H., Zhang Y., Sun Z., 2019. Recycling of spent lithium-ion batteries in view of lithium recovery: A critical review, J Clean Prod, vol. 228. pp. 801-813. doi: 10.1016/j.jclepro.2019.04.304

Liu F., Peng C., Porvali A., Wang Z., Wilson B. P., Lundström M., 2019. Synergistic recovery of valuable metals from spent nickel-metal hydride batteries and lithium-ion batteries, ACS Sustain Chem Eng, vol. 7:19. pp. 16103-16111. DOI: 10.1021/acssuschemeng.9b02863

Lupi C., Pilone D., 2000. Reductive stripping in vacuum of Fe(III) from D2EHPA, Hydrometallurgy, vol. 57:3. pp. 201-207. DOI: 10.1016/S0304-386X(00)00112-2

Metso, 2023. HSC Chemistry. Available at: https://www.hsc-chemistry.com/ [Accessed 13. September 2023]

Meshram P., Abdilash, Pandey B. D., Mankhand T. R., Deveci H., 2016. Comparison of different reductants in leaching of spent lithium ion batteries, JOM, vol. 68. pp. 2613-2623. DOI: 10.1007/s11837-016-2032-9

Mohr M., Peters J. F., Baumann M., Weil M., 2020. Toward a cell-chemistry specific life cycle assessment of lithium-ion battery recycling processes, J Indust Ecol, vol. 24:6, pp. 1310-1322. DOI: 10.1111/jiec.13021

Nowak M., Jaroszek H., Turkowaska, M., 2014. Conversion of waste sodium sulfate with bipolar membrane electrodialysis, in M. Bodzek, J. Pelczar, eds Monographs of the Environmental Engineering Committee Polish Academy of Sciences: Membranes and Membrane Processes in Environmental Protection, vol. 119. Warsaw: Polska Akademia Nauk. Komitet Inżynierii Środowiska. pp. 337-349.

Ogendengbe A., Achiobu K., Scoccimarro S., Brunet S., Fabrik M., Ibrahim H., 2020. Valorization of sodium sulfate waste to potassium sulfate fertilizer: experimental studies, process modeling, and optimization, Int J Green Energy, vol. 17:8. pp. 521-528. doi: 10.1080/15435085.2020.1763361

Peng C., Chang C., Wang Z., Wilson B. P., Liu F., Lundström M., 2019. Recovery of high-purity MnO_2 from the acid leaching solution of spent Li-ion batteries, JOM, vol. 72. pp. 790-799. DOI: 10.1007/s11837-019-03785-1

Porvali A., Chernyaev A., Shukla S., Lundström M., 2020a. Lithium ion battery active material dissolution kinetics in Fe(II)/Fe(III) catalyzed Cu-H_2SO_4 leaching system, Sep Purif Technol, vol. 236. DOI: 10.1016/j.seppur.2019.116305

Porvali A., Shukla S., Lundström M., 2020b. Low-acid leaching of lithium-ion battery active materials in Fe-catalyzed Cu-H_2SO_4 system, Hydrometallurgy, vol. 195. DOI: 10.1016/j.hydromet.2020.105408

Rey I., Vallejo C., Santiago G., Iturrondobeitia M., Lizundia E., 2021. Environmental impacts of graphite recycling from spent lithium-ion batteries based on life cycle assessment, ACS Sustainable Chemistry and Engineering, vol. 9:43. pp. 14488-14501. doi: 10.1021/acssuschemeng.1c04938

Rinne M., Elomaa H., Porvali A., Lundström M., 2021. Simulation-based life cycle assessment for hydrometallurgical recycling of mixed LIB and NiMH waste, Resour Conserv Recycl, vol. 170. DOI: 10.1016/j.resconrec.2021.105586

Schade W.E., Haug I., Berthold D., 2022. The future of the automotive sector: Emerging battery value chains in Europe. ETUI Research Paper – Report 2022.02. doi: 10.2139/ssrn.4220540

Singh D. K., Yadav K. K., Singh H., 2013. Extraction and stripping behavior of iron (III) from phosphoric acid medium by D2EHPA alone and its mixtures with TBP/TOPO, Sep Purif Technol, vol. 48:10. DOI: 10.1080/01496395.2012.753084

Sun L., Qiu K., 2011. Vacuum pyrolysis and hydrometallurgical process for the recovery of valuable metals from spent lithium-ion batteries, J Hazard Mater, vol. 194. pp. 378-384. DOI: 10.1016/j.jhazmat.2011.07.114

Tuovinen T., Tynjälä P., Vielma T., Lassi U., 2021. Utilization of waste sodium sulfate from battery chemical production in neutral electrolytic pickling, J Clean Prod, vol. 324. doi: 10.1016/j.jclepro.2021.129237

Szepessy S., Thorwid P., 2018. Low energy consumption of high-speed centrifuges, Chem Eng Technol, vol. 41:12. pp. 2375-2384. DOI: 10.1002/ceat.201800292

Zhang W., Singh P., Muir D., 2002. Oxidative precipitation of manganese with SO2/O2 and separation from cobalt and nickel, Hydrometallurgy, vol. 63:2. pp. 127-135. DOI: 10.1016/S0304-386X(01)00205-5

Zheng R., Zhao L., Wang W., Liu Y., Ma Q., Mu D., Li R., Dai C., 2016. Optimized Li and Fe recovery from spent lithium-ion batteries via a solution-precipitation method, RSC Advances, vol. 6:49. pp. 43613-43625. doi: 10.1039/C6RA05477C

Zubi G., Dufo-López R., Carvalho M., Pasaoglu G., 2018. The lithium-ion battery: state of the art and future perspectives, Renew Sustain Energy Rev, vol. 89. pp. 292-308. DOI: 10.1016/j.rser.2018.03.002

Wang W., Wu Y., 2017. An overview of recycling and treatment of spent $LiFePO_4$ batteries in China, Resour Conserv Recycl, vol. 127, pp. 233-243. DOI: 10.1016/j.resconrec.2017.08.019

S5. Unit specific and NMC material LCI

Table S5. Detailed LCI on process stages per 1 kg black mass, note that energy is in "kJ", and some flows are in grams (g) rather than kilograms. Solid wastes are calculated without moisture, which is counted towards the wastewater.

Inflows	***FS1***	***FS2***	***FS3***	***FS2-LA***	**Outflows**	***FS1***	***FS2***	***FS3***	***FS2-LA***
Leaching									
Black mass (kg)	1.00	1.00	1.00	1.00	Leach residue (kg)	0.60	0.60	0.60	0.60
Water (kg)	9.91	9.91	9.91	9.64	Wastewater (kg)	0.23	0.23	0.23	0.23
Electricity (kJ)	80.19	80.19	80.19	143.64					
Sulfuric acid (kg)	1.88	1.88	1.88	0.70					
Copper scrap (g)	60.22	60.22	60.22	70.72					
Cu removal									
Electricity (kJ)	20.08	20.08	20.08	17.73	NA				
Fe scrap (g)	71.09	71.09	71.09	67.66					
Fe and Al removal									
Electricity (kJ)	11.40	37.25	36.74	35.47	Solid residues (kg)	0.12	0.17	0.16	0.15
Oxygen (g)	41.70	38.31	57.23	33.98	Wastewater (g)	41.53	56.43	53.38	50.53
Caustic soda (kg)	0.14	1.03	1.03	0.13					
Manganese SX									
Water (kg)	3.45	1.45	-	1.50	NA				
Sulfuric acid (kg)	0.12	0.10	-	0.10					

Hydrochloric acid (kg)	0.13	-	-	-					
Caustic soda (kg)	1.04	0.03	-	0.03					
Kerosene (kg)	0.43	0.39	-	0.40					
D2EHPA (kg)	0.06	0.06	-	0.05					
Manganese oxidation									
Water (g)	46.27	45.14	52.94	41.16	Manganese oxide (g)	23.85	23.26	23.26	21.21
Electricity (kJ)	9.46	18.58	12.89	18.44	Impurities (g)	1.77	0.71	10.87	0.71
Oxygen (g)	13.17	12.84	15.06	11.71	Wastewater (g)	8.54	7.99	11.38	7.31
Sulfur dioxide (g)	1.68	1.64	1.93	1.50					
Caustic soda (g)	86.64	81.79	34.58	75.76					
Co and Ni SX									
Water (kg)	7.96	7.18	7.34	6.76	NA				
Sulfuric acid (kg)	0.90	0.83	0.85	0.78					
Caustic soda (kg)	0.74	0.68	0.70	0.63					
Kerosene (kg)	0.72	0.64	0.55	0.60					
D2EHPA (kg)	0.08	0.09	0.08	0.09					
Cyanex 272 (kg)	0.14	0.10	0.11	0.10					
Co and Ni crystallization									
Electricity (kJ)	263.12	236.91	240.73	223.01	Cobalt sulfate (g)	876.83	858.77	824.42	774.49
Steam (kJ)	1276.52	1064.83	1216.39	1279.30	Nickel sulfate (g)	126.52	124.04	121.40	111.22
					Impurities (g)	1.43	1.36	1.57	1.25
Li crystallization									
Electricity (kJ)	903.91	856.27	774.46	652.60	Lithium carbonate (g)	128.43	126.24	126.33	118.85
Steam (kJ)	4489.45	4076.09	3536.08	3789.06	Impurities (g)	1.18	0.92	1.64	1.13
Caustic soda (g)	0.79	0.75	0.72	0.39	Glauber salt (kg)	3.54	3.46	3.28	1.76
Soda (g)	184.22	181.08	181.20	170.48	Wastewater (kg)	0.89	0.87	0.83	0.44
Effluent treatment									
Electricity (kJ)	138.58	155.45	138.54	156.88	Solid residues (g)	72.48	86.32	92.56	47.38
Quicklime (g)	17.40	17.80	19.01	7.17	Wastewater (kg)	16.40	13.70	13.73	15.38
General									
Electricity (kJ)	360.00	360.00	360.00	360.00	Sulfate to water (g)	63.97	45.84	71.09	30.54
					Chloride to water (g)	123.35	-	-	-
					Cobalt to water (mg)	159.85	209.68	176.64	219.68
					Nickel to water (mg)	31.76	38.29	31.73	37.97
					Manganese to water (mg)	22.03	27.44	24.91	28.36
					Copper to water (mg)	0.22	0.28	0.27	0.30
					Iron to water (mg)	0.06	0.07	0.07	0.07

Table S6. The life cycle inventories for NMC chemistries, all are modeled with *FS2*.

Inflows	**NMC111**	**NMC532**	**NMC811**	**Unit**
Black mass	1.00	1.00	1.00	kg
Electricity, EU2020	1.66	1.66	1.63	MJ
Steam, chemical industry	4.83	4.85	4.79	MJ
Deionized water	10.17	10.18	9.25	kg
Sulfuric acid	2.86	2.87	2.87	kg
Caustic soda	1.78	1.79	1.78	kg
Lime, as quicklime	18.00	18.00	17.93	g
Sodium carbonate	180.02	180.50	180.77	g
Copper scrap	60.22	60.22	60.22	g
Iron scrap	76.66	76.66	76.66	g
Sulfur dioxide, liquid	7.72	6.94	2.31	g
Oxygen, liquid	98.42	92.49	56.28	g
Kerosene	1.09	1.09	1.04	kg
D2EHPA	0.16	0.16	0.16	kg
Cyanex 272	0.10	0.10	0.10	kg
Outflows	**NMC111**	**NMC532**	**NMC811**	**Unit**
Lithium carbonate	125.66	125.84	126.03	g
Cobalt sulfate	348.50	205.88	98.47	g
Nickel sulfate	326.87	492.54	790.32	g
Manganese dioxide	109.21	98.40	32.80	g
Solid waste	0.94	0.94	0.92	kg
Glauber salt	3.66	3.65	3.56	kg
Wastewater	16.20	16.23	15.34	kg
Sulfate to freshwater	47.43	47.17	46.41	g
Cobalt(II) (aq) to freshwater	117.61	91.91	68.19	mg
Nickel(II) (aq) to freshwater	77.52	108.19	164.53	mg
Copper(II) (aq) to freshwater	0.28	0.28	0.28	mg

S6. Tabulated numerical results

S6.1. Impact characterization

Table S7. Process and net impacts of the flowsheets.

	FS1		FS2		FS3		FS2-LA	
	Process	**Net**	**Process**	**Net**	**Process**	**Net**	**Process**	**Net**
CED (MJ)	249.63	-980.37	201.09	-1004.83	161.47	-998.53	135.96	-1066.02
ADPe (kg Sb-eq)	1.58 E-4	-46.08 E-4	1.17 E-4	-45.51 E-4	1.04 E-4	-43.86 E-4	0.68 E-4	-46.00 E-4
ADPf (MJ)	186.37	-158.83	155.35	-182.79	117.95	-207.05	105.11	-233.05
AP (kg SO_2-eq)	6.68 E-2	-16.95 E-2	5.73 E-2	-17.42 E-2	5.14 E-2	-17.16 E-2	3.60 E-2	-19.53 E-2
EP (kg PO_4-eq)	2.33 E-2	-3.77 E-2	1.87 E-2	-4.11 E-2	1.46 E-2	-4.31 E-2	1.22 E-2	-4.76 E-2
GWP (kg CO_2-eq)	7.96	-14.50	6.22	-15.79	5.44	-15.76	4.42	-17.58
HTP (kg DCB-eq)	8.74	-62.52	6.71	-63.09	5.89	-61.21	4.20	-65.60
ODP (kg R11-eq)	3.70 E-6	0.94 E-6	2.68 E-6	-0.02 E-6	2.18 E-6	-0.42 E-6	1.50 E-6	-1.21 E-6
POCP (kg Ethene-eq)	4.66 E-3	-7.73 E-3	3.91 E-3	-8.23 E-3	3.41 E-3	-8.29 E-3	2.66 E-3	-9.46 E-3

Table S8. Impact characterization of the NMC-feed sensitivity analyses.

	NMC 111		NMC 532		NMC 811	
	Process	**Net**	**Process**	**Net**	**Process**	**Net**
CED (MJ)	205.42	-377.03	205.63	-233.12	201.95	-174.77
ADPe (kg Sb-eq)	1.17 E-4	-21.24 E-4	1.18 E-4	-15.74 E-4	1.17 E-4	-13.48 E-4
ADPf (MJ)	160.12	-9.16	160.21	30.95	157.19	46.24
AP (kg SO_2-eq)	5.87 E-2	-7.11 E-2	5.88 E-2	-5.37 E-2	5.81 E-2	-5.90 E-2
EP (kg PO_4-eq)	1.92 E-2	-1.35 E-2	1.92 E-2	-0.72 E-2	1.91 E-2	-0.48 E-2
GWP (kg CO_2-eq)	6.29	-4.78	6.29	-2.13	6.23	-0.88
HTP (kg DCB-eq)	6.79	-28.49	6.80	-20.82	6.77	-18.23
ODP (kg R11-eq)	2.70 E-6	1.39 E-6	2.71 E-6	1.73 E-6	2.67 E-6	1.85 E-6
POCP (kg Ethene-eq)	4.00 E-3	-2.75 E-3	4.01 E-3	-1.79 E-3	3.97 E-3	-2.00 E-3

S6.2. Contribution analysis (units)

Table S9. Contribution analyses by unit level.

CED	**FS1 (%)**	**FS2 (%)**	**FS3 (%)**	**FS2-LA (%)**
Leaching	2.83	3.51	4.37	1.61
Copper cementation	0.04	0.05	0.06	0.05
Iron removal	8.37	10.24	12.94	1.82
Manganese SX	25.70	20.19	-	22.00
Manganese precipitation	0.77	0.92	0.59	1.05
Cobalt and nickel SX	52.86	57.16	68.83	64.68
Cobalt and nickel crystallization	1.19	1.26	1.75	1.67
Lithium carbonate precipitation	4.57	5.23	5.77	5.47
Effluent treatment	0.17	0.24	0.27	0.24
Auxiliary equipment	3.50	1.21	5.41	1.41
Credits	-493.97	-599.70	-718.39	-696.42
ADPe	**FS1 (%)**	**FS2 (%)**	**FS3 (%)**	**FS2-LA (%)**
Leaching	7.87	10.60	11.90	6.04
Copper cementation	0.14	0.19	0.21	0.27
Iron removal	20.32	27.38	30.75	5.30
Manganese SX	29.82	10.31	-	13.43
Manganese precipitation	1.73	2.21	1.08	3.11
Cobalt and nickel SX	36.16	44.73	50.21	65.34
Cobalt and nickel crystallization	0.08	0.09	0.11	0.15
Lithium carbonate precipitation	3.19	4.20	4.67	5.91
Effluent treatment	0.03	0.04	0.04	0.06
Auxiliary equipment	0.68	0.25	1.03	0.38
Credits	-3025.08	-3994.69	-4314.58	-6053.35
ADPf	**FS1 (%)**	**FS2 (%)**	**FS3 (%)**	**FS2-LA (%)**
Leaching	2.99	3.59	4.73	1.56
Copper cementation	0.03	0.03	0.04	0.03
Iron removal	6.08	7.21	9.58	1.22
Manganese SX	26.13	22.44	-	23.93
Manganese precipitation	0.56	0.64	0.43	0.71
Cobalt and nickel SX	56.33	58.91	74.28	64.71
Cobalt and nickel crystallization	1.23	1.25	1.86	1.65
Lithium carbonate precipitation	4.71	5.19	6.03	5.37
Effluent treatment	0.11	0.14	0.18	0.13
Auxiliary equipment	1.82	0.61	2.87	0.69
Credits	-185.22	-217.66	-275.53	-246.25
AP	**FS1 (%)**	**FS2 (%)**	**FS3 (%)**	**FS2-LA (%)**
Leaching	27.50	32.00	35.68	16.92
Copper cementation	0.03	0.04	0.04	0.05

Iron removal	6.81	7.84	8.84	1.60
Manganese SX	16.98	10.52	-	13.83
Manganese precipitation	0.77	0.86	0.61	1.16
Cobalt and nickel SX	43.31	44.36	49.49	60.48
Cobalt and nickel crystallization	0.63	0.61	0.77	1.02
Lithium carbonate precipitation	3.18	3.46	3.52	4.52
Effluent treatment	0.06	0.07	0.08	0.07
Auxiliary equipment	0.74	0.24	0.97	0.34
Credits	-353.89	-404.31	-434.26	-571.39
EP	**FS1 (%)**	**FS2 (%)**	**FS3 (%)**	**FS2-LA (%)**
Leaching	2.10	2.61	3.35	1.24
Copper cementation	0.04	0.05	0.06	0.05
Iron removal	11.65	14.33	18.57	2.57
Manganese SX	30.83	20.66	-	21.82
Manganese precipitation	1.06	1.25	0.81	1.49
Cobalt and nickel SX	50.56	57.56	71.69	68.75
Cobalt and nickel crystallization	0.39	0.41	0.59	0.58
Lithium carbonate precipitation	2.29	2.68	3.19	2.99
Effluent treatment	0.06	0.08	0.09	0.08
Auxiliary equipment	1.03	0.36	1.64	0.43
Credits	-261.91	-319.66	-395.46	-388.74
GWP	**FS1 (%)**	**FS2 (%)**	**FS3 (%)**	**FS2-LA (%)**
Leaching	2.56	3.28	3.74	1.60
Copper cementation	0.04	0.06	0.06	0.06
Iron removal	10.83	13.69	15.85	2.44
Manganese SX	22.50	14.19	-	15.04
Manganese precipitation	0.98	1.20	0.70	1.42
Cobalt and nickel SX	50.80	55.52	63.77	65.60
Cobalt and nickel crystallization	1.87	2.01	2.59	2.85
Lithium carbonate precipitation	7.30	8.60	8.70	9.47
Effluent treatment	0.36	0.48	0.55	0.34
Auxiliary equipment	2.75	0.98	4.03	1.18
Credits	-282.18	-353.92	-389.80	-426.19
HTP	**FS1 (%)**	**FS2 (%)**	**FS3 (%)**	**FS2-LA (%)**
Leaching	7.92	10.32	11.76	1.25
Copper cementation	0.14	0.19	0.21	0.07
Iron removal	15.46	19.98	22.94	1.03
Manganese SX	26.46	12.26	-	4.16
Manganese precipitation	1.35	1.67	0.88	0.61
Cobalt and nickel SX	43.17	49.79	56.69	18.59
Cobalt and nickel crystallization	0.38	0.43	0.54	0.19
Lithium carbonate precipitation	3.47	4.32	4.69	1.53
Effluent treatment	0.36	0.58	0.38	72.39
Auxiliary equipment	1.29	0.47	1.92	0.18

Credits	-815.25	-1040.77	-1139.95	-401.05
ODP	**FS1 (%)**	**FS2 (%)**	**FS3 (%)**	**FS2-LA (%)**
Leaching	0.61	0.84	1.04	0.52
Copper cementation	0.01	0.02	0.02	0.02
Iron removal	21.77	30.01	36.96	5.44
Manganese SX	34.82	15.73	-	21.60
Manganese precipitation	1.84	2.40	1.26	3.18
Cobalt and nickel SX	38.09	47.94	56.50	65.01
Cobalt and nickel crystallization	0.48	0.55	0.77	0.93
Lithium carbonate precipitation	1.76	2.23	2.41	2.91
Effluent treatment	0.05	0.07	0.09	0.07
Auxiliary equipment	0.56	0.22	0.96	0.31
Credits	-74.52	-100.65	-119.38	-144.16
POCP	**FS1 (%)**	**FS2 (%)**	**FS3 (%)**	**FS2-LA (%)**
Leaching	16.41	19.58	22.44	9.24
Copper cementation	0.04	0.05	0.05	0.05
Iron removal	5.76	6.81	7.89	1.23
Manganese SX	18.05	13.48	-	15.51
Manganese precipitation	0.61	0.69	0.47	0.84
Cobalt and nickel SX	54.52	55.09	63.52	67.94
Cobalt and nickel crystallization	0.66	0.66	0.86	0.98
Lithium carbonate precipitation	2.88	3.18	3.28	3.68
Effluent treatment	0.12	0.15	0.17	0.11
Auxiliary equipment	0.96	0.32	1.31	0.40
Credits	-265.72	-310.50	-343.08	-391.41

S6.3. Contribution analysis (flows)

Table S10. Contribution analysis on flow level (%).

CED	**FS1 (%)**	**FS2 (%)**	**FS3 (%)**	**FS2-LA (%)**
Electricity	1.61	0.66	2.30	0.53
Copper scrap	-0.01	0.00	-0.01	-0.01
Direct impacts	0.00	0.00	0.00	0.00
Caustic soda (NaOH)	14.78	5.70	20.93	31.77
Steam	3.84	1.41	5.32	0.22
Hydrochloric acid (HCl)	0.73	0.00	0.00	0.00
Iron scrap	0.02	0.01	0.03	0.26
Oxygen, liquid (O_2)	0.35	0.14	0.56	0.08
Quicklime (CaO)	0.04	0.02	0.07	0.00
Sulfur dioxide, liquid (SO_2)	0.01	0.00	0.01	0.03
Sulfuric acid (H_2SO_4)	4.21	1.73	6.09	13.36
Soda (Na_2CO_3)	0.38	0.16	0.58	5.47
Water softening	0.04	0.01	0.04	0.07
Organics	74.01	90.17	64.08	48.22
ADPe	**FS1 (%)**	**FS2 (%)**	**FS3 (%)**	**FS2-LA (%)**

Electricity	0.31	0.37	0.44	0.53
Copper scrap	0.00	0.00	0.00	-0.01
Direct impacts	0.00	0.00	0.00	0.00
Caustic soda (NaOH)	37.58	41.95	52.08	31.77
Steam	0.12	0.13	0.16	0.22
Hydrochloric acid (HCl)	2.15	0.00	0.00	0.00
Iron scrap	0.13	0.16	0.20	0.26
Oxygen, liquid (O_2)	0.05	0.06	0.08	0.08
Quicklime (CaO)	0.00	0.00	0.00	0.00
Sulfur dioxide, liquid (SO_2)	0.01	0.02	0.02	0.03
Sulfuric acid (H_2SO_4)	12.06	14.32	17.10	13.36
Soda (Na_2CO_3)	2.89	3.48	4.30	5.47
Water softening	0.05	0.04	0.05	0.07
Organics	44.65	39.47	25.56	48.22
ADPf	**FS1 (%)**	**FS2 (%)**	**FS3 (%)**	**FS2-LA (%)**
Electricity	0.84	0.26	1.22	0.95
Copper scrap	-0.01	0.00	-0.02	-0.02
Direct impacts	0.00	0.00	0.00	0.00
Caustic soda (NaOH)	10.79	3.20	15.68	6.07
Steam	4.51	1.27	6.38	5.38
Hydrochloric acid (HCl)	0.60	0.00	0.00	0.00
Iron scrap	0.02	0.01	0.03	0.02
Oxygen, liquid (O_2)	0.23	0.07	0.37	0.26
Quicklime (CaO)	0.04	0.01	0.07	0.02
Sulfur dioxide, liquid (SO_2)	0.01	0.00	0.01	0.01
Sulfuric acid (H_2SO_4)	4.53	1.42	6.71	3.35
Soda (Na_2CO_3)	0.37	0.12	0.58	0.47
Water softening	0.03	0.01	0.03	0.03
Organics	78.06	93.63	68.92	83.47
AP	**FS1 (%)**	**FS2 (%)**	**FS3 (%)**	**FS2-LA (%)**
Electricity	0.34	0.32	0.41	0.47
Copper scrap	-0.01	-0.01	-0.01	-0.01
Direct impacts	0.00	0.00	0.00	0.00
Caustic soda (NaOH)	12.19	10.90	14.53	8.33
Steam	2.34	2.00	2.73	3.38
Hydrochloric acid (HCl)	0.89	0.00	0.00	0.00
Iron scrap	0.03	0.03	0.04	0.05
Oxygen, liquid (O_2)	0.21	0.20	0.29	0.29
Quicklime (CaO)	0.03	0.03	0.04	0.02
Sulfur dioxide, liquid (SO_2)	0.16	0.15	0.24	0.24
Sulfuric acid (H_2SO_4)	42.38	40.24	51.61	38.05
Soda (Na_2CO_3)	0.97	0.94	1.24	1.49
Water softening	0.03	0.02	0.03	0.04
Organics	40.43	45.18	28.86	47.67

EP	**FS1 (%)**	**FS2 (%)**	**FS3 (%)**	**FS2-LA (%)**
Electricity	0.48	0.21	0.70	0.60
Copper scrap	-0.01	0.00	-0.01	-0.01
Direct impacts	0.00	0.00	0.00	0.00
Caustic soda (NaOH)	20.74	8.63	30.29	13.02
Steam	1.29	0.51	1.85	1.72
Hydrochloric acid (HCl)	2.92	0.00	0.00	0.00
Iron scrap	0.03	0.01	0.05	0.04
Oxygen, liquid (O_2)	0.45	0.19	0.74	0.56
Quicklime (CaO)	0.02	0.01	0.03	0.01
Sulfur dioxide, liquid (SO_2)	0.01	0.00	0.01	0.01
Sulfuric acid (H_2SO_4)	3.14	1.39	4.70	2.60
Soda (Na_2CO_3)	0.91	0.41	1.42	1.27
Water softening	0.06	0.02	0.06	0.06
Organics	69.97	88.62	60.16	80.12
GWP	**FS1 (%)**	**FS2 (%)**	**FS3 (%)**	**FS2-LA (%)**
Electricity	1.27	0.72	1.71	1.62
Copper scrap	-0.01	-0.01	-0.02	-0.02
Direct impacts	0.00	0.00	0.00	0.00
Caustic soda (NaOH)	19.22	10.37	25.74	12.28
Steam	6.82	3.50	8.95	9.26
Hydrochloric acid (HCl)	0.93	0.00	0.00	0.00
Iron scrap	0.03	0.02	0.04	0.04
Oxygen, liquid (O_2)	0.40	0.22	0.61	0.51
Quicklime (CaO)	0.26	0.15	0.41	0.16
Sulfur dioxide, liquid (SO_2)	0.01	0.00	0.01	0.01
Sulfuric acid (H_2SO_4)	3.79	2.17	5.22	3.20
Soda (Na_2CO_3)	0.74	0.43	1.06	1.05
Water softening	0.06	0.03	0.05	0.06
Organics	66.49	82.41	56.20	71.83
HTP	**FS1 (%)**	**FS2 (%)**	**FS3 (%)**	**FS2-LA (%)**
Electricity	0.59	0.53	0.81	0.25
Copper scrap	-0.65	-0.60	-0.96	-0.38
Direct impacts	0.30	0.35	0.47	0.19
Caustic soda (NaOH)	28.26	23.74	38.39	5.86
Steam	1.19	0.95	1.58	0.52
Hydrochloric acid (HCl)	1.82	0.00	0.00	0.00
Iron scrap	0.14	0.13	0.20	0.06
Oxygen, liquid (O_2)	0.21	0.18	0.33	0.09
Quicklime (CaO)	0.01	0.01	0.02	0.00
Sulfur dioxide, liquid (SO_2)	0.02	0.01	0.03	0.01
Sulfuric acid (H_2SO_4)	13.04	11.71	18.18	3.58
Soda (Na_2CO_3)	2.11	1.91	3.07	0.98
Water softening	0.07	0.05	0.07	0.02

Organics	52.90	61.03	37.81	88.81
ODP	**FS1 (%)**	**FS2 (%)**	**FS3 (%)**	**FS2-LA (%)**
Electricity	0.26	0.25	0.40	0.42
Copper scrap	-0.01	-0.01	-0.01	-0.01
Direct impacts	0.00	0.00	0.00	0.00
Caustic soda (NaOH)	40.29	36.90	62.91	32.84
Steam	1.79	1.56	2.72	3.10
Hydrochloric acid (HCl)	1.35	0.00	0.00	0.00
Iron scrap	0.01	0.01	0.01	0.02
Oxygen, liquid (O_2)	0.04	0.03	0.06	0.06
Quicklime (CaO)	0.03	0.03	0.05	0.02
Sulfur dioxide, liquid (SO_2)	0.00	0.00	0.00	0.00
Sulfuric acid (H_2SO_4)	0.85	0.83	1.35	0.92
Soda (Na_2CO_3)	0.07	0.07	0.12	0.13
Water softening	0.06	0.05	0.07	0.09
Organics	55.26	60.28	32.31	62.42
POCP	**FS1 (%)**	**FS2 (%)**	**FS3 (%)**	**FS2-LA (%)**
Electricity	0.44	0.27	0.56	0.56
Copper scrap	-0.02	-0.01	-0.02	-0.03
Direct impacts	0.00	0.00	0.00	0.00
Caustic soda (NaOH)	10.34	5.99	12.96	6.43
Steam	2.42	1.33	2.96	3.19
Hydrochloric acid (HCl)	0.71	0.00	0.00	0.00
Iron scrap	0.03	0.02	0.05	0.05
Oxygen, liquid (O_2)	0.17	0.10	0.25	0.22
Quicklime (CaO)	0.08	0.05	0.12	0.05
Sulfur dioxide, liquid (SO_2)	0.09	0.06	0.15	0.13
Sulfuric acid (H_2SO_4)	25.31	15.55	32.25	20.74
Soda (Na_2CO_3)	0.56	0.35	0.74	0.78
Water softening	0.03	0.01	0.02	0.03
Organics	59.83	76.27	49.96	67.86